INTERNATIONAL JOURNAL FOR NUMERICAL METHODS IN FLUIDS
Int. J. Numer. Meth. Fluids 2005; **47**:561–574
Published online 14 December 2004 in Wiley InterScience (www.interscience.wiley.com). DOI: 10.1002/fld.831

Advanced numerical simulation of heat transfer problems

Masahiro Ikegawa[1,*,†], Masayuki Kaiho[2] and Atsushi Hayasaka[1]

[1]*Division of Mechanical Science, Graduate School of Engineering, Hokkaido University, N13 W8, Kita-ku, Sapporo, 060-8628, Japan*
[2]*Mechanical Engineering Research Laboratory, Hitachi, Ltd., 502, Kandatsu, Tsuchiura, Ibaraki, 300-0013, Japan*

SUMMARY

This paper describes two kinds of practical numerical techniques for heat transfer problems. One is a parallel large eddy simulation technique with heat transfer using tetrahedral finite elements and the other is the Voxel method using a uniform grid combined with the discrete element method for liquid–solid two-phase flow problems. These two approaches are taken to be the candidates for the practical use of large-scale heat transfer analysis for various kinds of problems. The former can reduce the overall computing time in performing a large-scale heat transfer analysis through the combined use of an automatic mesh generation software, and the latter is very useful and efficient to analyse a complicated heat transfer phenomena such as a liquid–solid two-phase flow in a fluidized bed. Numerical examples for both approaches show fairly good agreement with experimental results and these two methods are demonstrated to be powerful tools for analysing large-scale and complicated heat transfer problems.

KEY WORDS: numerical heat transfer; finite element method; large eddy simulation; Voxel method; liquid–solid two-phase flow

1. INTRODUCTION

Owing to recent advances in computer capabilities, numerical analyses are now widely used in various kinds of design of manufacturing products and of investigation of complex phenomena. The important subjects for practical use of numerical analysis are development of numerical simulation system accompanied by a fully automatic mesh generation based on CAD data and a highly efficient numerical technique for very large-scale analysis. Two approaches may be considered as the candidates along this line. One is the finite element analysis using tetrahedral elements and the other is so called Voxel method using uniform orthogonal finite difference grids. In this paper, we examine the possibilities of these two approaches.

*Correspondence to: M. Ikegawa, Division of Mechanical Science, Graduate School of Engineering, Hokkaido University, N13 W8, Kita-ku, Sapporo, 060-8628, Japan.
†E-mail: ikega@agate.plata.or.jp, kawanami@eng.hokudai.ac.jp

Received 2 July 2003
Accepted 18 August 2004

Firstly, we present a parallel LES (large eddy simulation) for viscous incompressible flow with heat transfer based on the finite element method using tetrahedral elements. Due to the progress of Delaunay method [1] and other tetrahedral mesh generation techniques [2], it is easy to generate and control tetrahedral finite-element meshes for flow problems with complex geometries. A new algorithm based on the SIMPLER method [3] is proposed to solve the Navier–Stokes equations, in which BTD (balancing tensor diffusivity) [4] is introduced to ensure numerical stability. The Smagorinsky model is applied to approximate the Reynolds stress and the zero-equation model is employed to solve the energy equation. Parallelization of the code is based on the domain decomposition method and the recursive graph bisection algorithm [5] is used to reduce the communication time between processors. Numerical results for heat transfer problems in a rotating cavity are shown to demonstrate the effectiveness of the present method.

Secondly, we show a two-dimensional numerical simulation of fluidized beds based on the Voxel method combined with the discrete element method (DEM) [6], in which particle motion is calculated using ordinary Newton's equation of motion, modelling the contact forces by the DEM. For this kind of problems, Tezduyar *et al.* [7–9] analysed behaviour of multiple spheres falling in a liquid-filled tube based on a stabilized space-time finite element formulation. In our analysis, the locally averaged Navier–Stokes equations are solved to analyse the fluid motion, taking the interaction between fluid and particle into consideration. Flow and temperature fields are solved by the finite difference method with uniform grid size, the so-called Voxel method. Numerical results for a fluidized bed are also demonstrated.

Through these two analyses, both of the finite element method using tetrahedral elements and the voxel method using orthogonal uniform grids are shown to be powerful tools for practical large-scale heat transfer and fluid flow problems.

2. PARALLEL LARGE EDDY SIMULATION USING TETRAHEDRAL FINITE ELEMENTS

Here we introduce a three-dimensional parallel LES technique using tetrahedral finite element meshes for heat transfer problems.

2.1. Solution algorithm

The governing equations for viscous incompressible flow problems with heat transfer are given by the Navier–Stokes equations, equation of continuity and the energy equation, and are expressed in tensor form using summation conventions as follows:

$$\dot{U}_i + U_j U_{i,j} = -P_{,i}/\rho + \nu(U_{i,j} + U_{j,i})_{,j} \tag{1}$$

$$U_{i,i} = 0 \tag{2}$$

$$\dot{T} + (U_j T)_{,j} = \kappa T_{,ii} \tag{3}$$

where U_i is the velocity component in the x_i direction, P is the pressure, ρ is the density, ν is the kinematic viscosity, T is the temperature, κ is the thermal diffusivity and the superscripted

dot '·' indicates a time derivative. The boundary conditions for a flow field are given on the boundary $\Gamma(\Gamma = \Gamma_1 + \Gamma_2)$ as

$$U_i = \hat{U}_i \quad \text{on} \quad \Gamma_1 \tag{4}$$

$$P = 0, \quad n_j U_{i,j} = 0 \quad \text{on} \quad \Gamma_2 \tag{5}$$

where the hat indicates prescribed values and n_i is the direction cosine, with respect to the x_i axis, of the normal $\boldsymbol{n}$ drawn outward on the boundary Γ.

The fractional step method [10] accompanied by the correction term of the BTD [4] is used to solve the Navier–Stokes equations for the purpose of achieving the equal-order interpolation for the velocity and the pressure. By applying the implicit scheme to the prediction stage and applying the two-step correction of the SIMPLER procedure [3] to the correction stage, the following three-step scheme, in which the flow field is proceeded by a time increment Δt, is introduced to ensure an accurate and stable computation:

Step 1:

$$(\tilde{U}_i - U_i^n)/\Delta t = (1-\theta)F_i^n + \theta \tilde{F}_i \tag{6}$$

Step 2:

$$\phi_{,ii} = -\tilde{U}_{i,i} \tag{7}$$

$$P^{n+1} = -\phi/\rho\Delta t \tag{8}$$

$$U_i^* = \tilde{U}_i + \phi_{,i} \tag{9}$$

Step 3:

$$\varphi_{,ii} = -U_{i,i}^* \tag{10}$$

$$U_i^{n+1} = U_i^* + \varphi_{,i} \tag{11}$$

where

$$F_i^n = -U_j^n U_{i,j}^n + U_k^n (U_j^n U_{i,j}^n)_{,k} \Delta t/2 - \nu U_{i,jj}^n \tag{12}$$

where $\tilde{U}_i$ is the velocity for the prediction stage and ϕ, ψ are the potential functions for the first and the second correction, respectively. The second term of the right hand side of Equation (12) indicates the BTD term. In our analysis, θ is set to 0.5 as in the Crank–Nicholson method to avoid an excessive artificial diffusion.

The Galerkin method is employed for the finite-element formulations and the linear tetrahedral elements are used to discretize Equations (6)–(11). The parallel matrix solver is used to solve the linear equations defined by Equations (6), (7), and (10). To solve Equations (9) and (11), the elemental residuals are firstly calculated and then the elemental residuals are scattered to the nodal residuals using the lumped mass matrix.

In this study, the LES technique is applied to accurately simulate the turbulence. The governing equations for the LES are the filtered Navier–Stokes equations and the continuity

equation and are expressed in tensor form using summation conventions as follows:

$$\dot{\bar{U}}_i + \bar{U}_j \bar{U}_{i,j} = -\bar{P}_{,i}/\rho + \{\nu(\bar{U}_{i,j} + \bar{U}_{j,i}) - \overline{U_i' U_j'}\}_{,j} \tag{13}$$

$$\bar{U}_{i,j} = 0 \tag{14}$$

where $\bar{U}_i$ and $\bar{P}$ denote the grid-scale velocity component and the pressure, respectively, and $-\overline{U_i' U_j'}$ is the Reynolds stress. The Reynolds stress is modelled by the commonly used Smagorinsky model as follows:

$$-\overline{U_i' U_j'} = \nu_{\mathrm{SGS}}(\bar{U}_{i,j} + \bar{U}_{j,i}) - \delta_{ij}\overline{U_k' U_k'}/3 \tag{15}$$

$$\nu_{\mathrm{SGS}} = (C\Delta)^2(2\bar{S}_{ij}\bar{S}_{ij})^{0.5}; \quad \bar{S}_{ij} = (\bar{U}_{i,j} + \bar{U}_{j,i})/2 \tag{16}$$

where

$$\delta_{ij} = \begin{cases} 1 & (i = j) \\ 0 & (i \neq j) \end{cases} \tag{17}$$

where C is the Smagorinsky model constant set to a value of 0.15 in the present study and Δ is the representative element dimension which will be calculated from the volume of each finite element. By substituting Equation (15) into Equation (13), the following equation is obtained:

$$\dot{\bar{U}}_i + \bar{U}_j \bar{U}_{i,j} = -\bar{P}_{,i}/\rho + (\nu + \nu_{\mathrm{SGS}})(\bar{U}_{i,j} + \bar{U}_{j,i})_{,j} \tag{18}$$

Instead of solving Equation (1), we solve Equation (18) using the algorithm shown in Equations (6)–(11).

For the energy equation (3), various kinds of turbulence model have been proposed so far. In the present analysis, the following 0-equation model is employed:

$$\dot{T} + (U_j T)_{,j} = (\kappa + \kappa_{\mathrm{SGS}})T_{,ii}$$

$$\kappa_{\mathrm{SGS}} = \nu_{\mathrm{SGS}}/Pr_{\mathrm{SGS}} \tag{19}$$

where Pr_{SGS} is SGS Prantl number and is set to 0.4.

2.2. Numerical examples

To verify the effectiveness of the present method, we computed the natural convection problem in a cubic cavity as shown in Figure 1. We used the Hitachi SR2201 machine, which has 256 processor-nodes. Its peak performance is 300 Mflops in each processor giving a total of 76.8 Gflops. To accurately capture the boundary layer, we used the combination of Delaunay-type mesh generation for internal computational domain and the structured-type generation near the wall surface. The RGB (recursive graph bisection) method which has the merit on the partitioning CPU time and memory usage, was selected to partition the finite element meshes. Figure 2 is the mesh used in the analysis. Computations are carried out for the Rayleigh

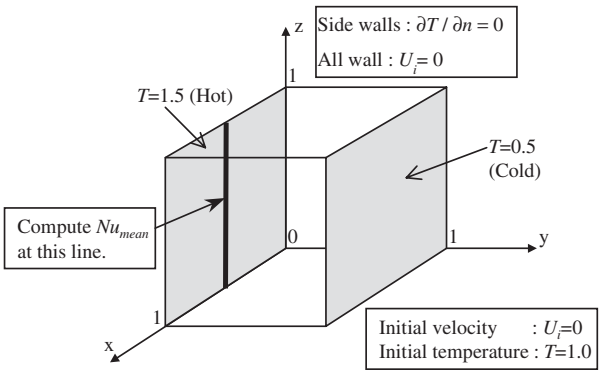

Figure 1. Analysis model and boundary conditions.

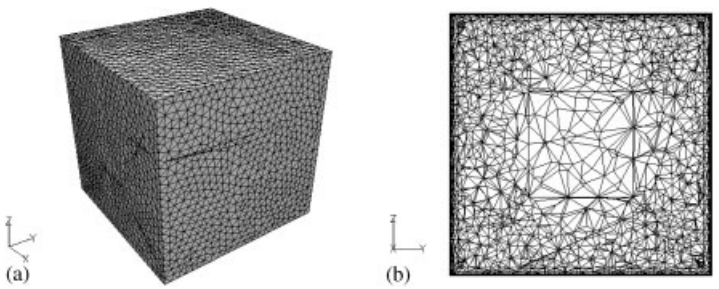

Figure 2. Global and sectional view of the mesh: (a) global view; and (b) sectional view.

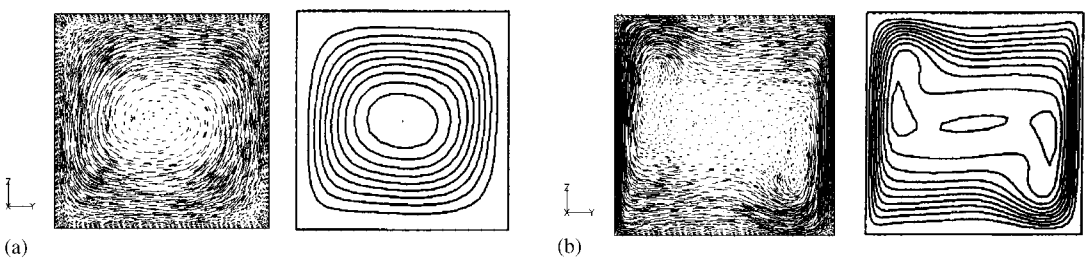

Figure 3. Velocity vectors computed by the present scheme (left) and streamline computed by De Vahl Davis [11] (right): (a) $Ra = 10^4$; and (b) $Ra = 10^6$.

number from 10^3 to 10^{10}. In Figures 3 and 4, we show the computed velocity vector and temperature profiles at $Ra = 10^4$ and 10^6 in the central cross section as shown in Figure 1. Figure 5 demonstrates the comparison of the mean Nusselt number at the hot wall between the present and conventional calculations. The present results showed good agreement with the results of De Vahl Davis [11] or Le Quere [12] and we were able to stably calculate the high Rayleigh number case ($Ra = 10^9$–10^{10}). We applied the present scheme to the heat transfer

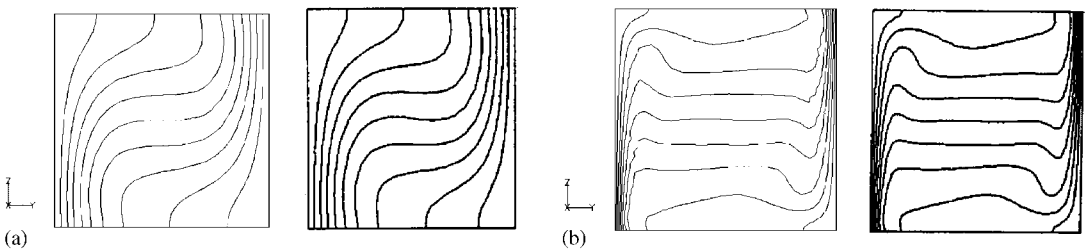

Figure 4. Temperature profiles computed by the present method (left) and by De Vahl Davis [11] (right): (a) $Ra = 10^4$; and (b) $Ra = 10^6$.

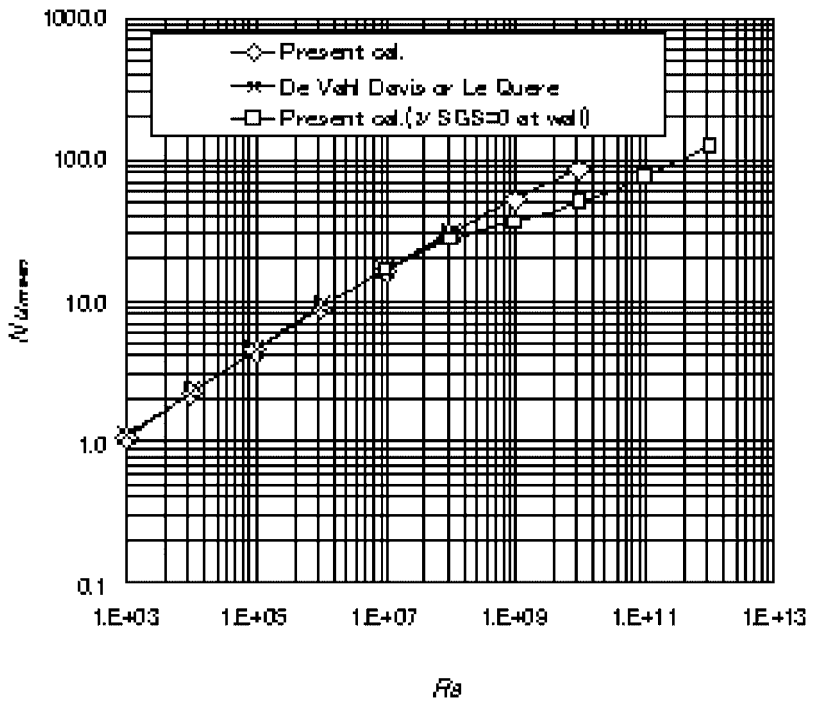

Figure 5. Computed mean Nusselt number on the hot wall in a cubic cavity.

problem in a rotating heated cavity, which often appears in the cooling of real products. Figure 6 shows a computational model and mesh. The computed velocity vectors in the cross section of a rotating cavity are shown in Figure 7, and the computed mean Nusselt number on a heated wall is shown in Figure 8. Numerical results showed good agreement with the experimental results.

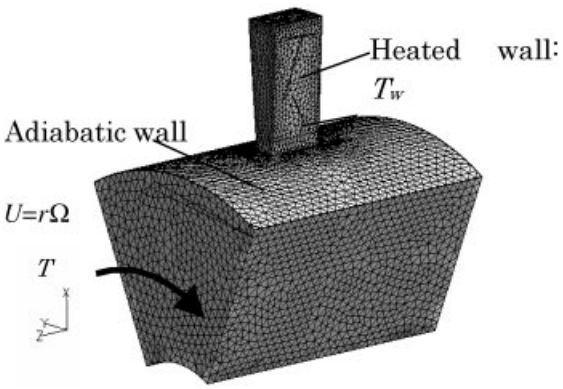

Figure 6. Analysis mesh and boundary conditions for a rotating cavity problem.

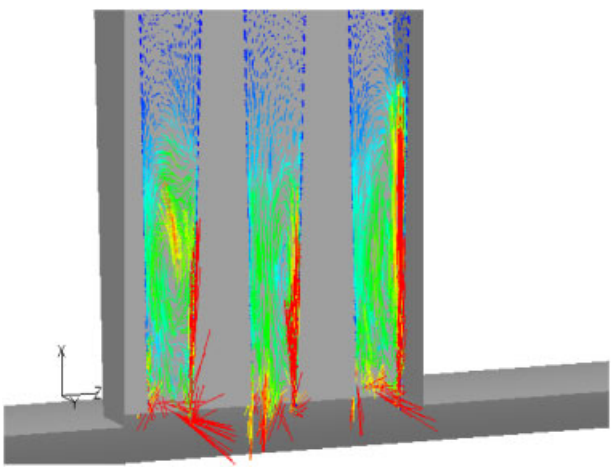

Figure 7. Close up of velocity vectors in a rotating cavity.

3. LIQUID–SOLID TWO-PHASE FLOW ANALYSIS BY THE VOXEL METHOD AND DISCRETE ELEMENT METHOD

Another possibility of practical large-scale heat transfer analysis is the use of Voxel method, in which a uniform orthogonal finite difference grid is employed. Here we show a two-dimensional numerical simulation of heat transfer and fluid flow problem in a solid–liquid fluidized bed as an example to demonstrate the effectiveness of this method. Advantages of the Voxel method are easy mesh generation and rapid convergence of the pressure equation. These advantages result in large reduction of analysis time in large-scale fluid flow and heat transfer analyses.

As is well-known, liquid–solid fluidized beds show excellent heat transfer characteristics due to mixing a flow field by moving particles, and attract many attentions for a design

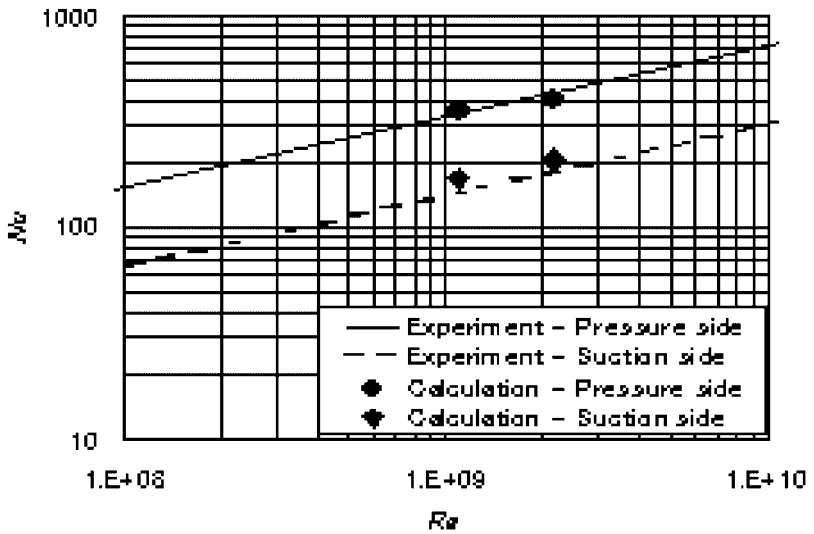

Figure 8. Comparison of Nusselt number.

of a high-performance heat exchanger. Although the hydrodynamic mechanism of liquid–solid fluidization has been extensively studied by several researchers, the research on heat and mass transfer problems still remain largely empirical, especially for liquid–solid fluidized beds. Recently, flow analysis using the discrete element method, in which solid particle motion is calculated based on ordinary Newton's equation of motion, modelling the contact forces by the DEM [6,13]. However, this approach is limited to the flow analysis in gas–solid fluidized beds so far. In what follows, we propose a Voxel method combined with the DEM and apply the method to flow and heat transfer analysis in a liquid–solid fluidized bed with particles of a little small density compared with the working fluid.

3.1. Governing equations

Fluid flow in a fluidized bed is a very complicated flow through moving particles from a microscopic point of view and is difficult to permit direct solution. Therefore we employ the following equations which are originally developed by Anderson and Jackson [14] and are obtained by locally averaging the Navier–Stokes equations over regions which contain particles but are still small compared with the scale of macroscopic variations from point to point in the system.

$$\dot{\varepsilon} + (\varepsilon u_i)_{,i} = 0 \tag{20}$$

$$\varepsilon \dot{u} + (\varepsilon u_i u_j)_{,j} = -\varepsilon p_{,i}/\rho + \varepsilon \nu u_{i,jj} + f_i \tag{21}$$

$$\varepsilon \rho c_p (\dot{T} + u_i T_{,i}) = (\lambda \varepsilon T)_{,ii} \tag{22}$$

In the above equations, ε is the local mean void fraction, u_i and p are the local mean velocity components and pressure, respectively, ρ is the density, c_p is the specific heat of the fluid

and T is the local mean temperature. The last term of Equation (21) is the interaction term between particles and fluid and is given by

$$f_i = \beta(v_{pi} - u_i)/\rho \tag{23}$$

where v_{pi} is the velocity component of a particle in x_i direction and drag coefficient β is given by

$$\beta = \begin{cases} \rho\nu(1-\varepsilon)\{150(1-\varepsilon) + 1.75Re\}/(d_p^2\varepsilon^2) & (\varepsilon \leqslant 0.8) \\ 0.75C_D\rho\nu(1-\varepsilon)\varepsilon^{-2.7}Re/d_p^2 & (\varepsilon \geqslant 0.8) \end{cases} \tag{24}$$

$$C_D = \begin{cases} 24(1 + 0.15Re^{0.687})/Re & (Re \leqslant 1000) \\ 0.43 & (Re \geqslant 1000) \end{cases} \tag{25}$$

$$Re = |\mathbf{v}_p - \bar{u}|\varepsilon d_p/\nu \tag{26}$$

where C_D is the drag coefficient for a sphere and Re is the Reynolds number with respect to each particle which is defined by a relative fluid velocity and the particle diameter. The maximum value of Re is around 1000 in our analyses.

In the present analysis, three kinds of grid, coarse grid, fine grid and particle grid, are used in order to make detailed numerical analysis in a fluidized bed with a heated cylinder as shown in Figure 9. The coarse grid is necessary for computing void fraction and interacting force between fluid and particles, because these values should be calculated by space averaging in a grid larger than a particle diameter. The detailed flow analysis is performed using a fine grid generated by dividing a coarse grid cell into several grids. Particle grid is to compute fluid forces acting on each particle and is formed by assembling several fine grids covered a region about two times larger than a particle diameter. Governing equations are solved by the SIMPLE algorithm [3].

3.2. Motion of particles

Many solid particles in a high-density solid–liquid two-phase flow such as in a fluidized bed are moved around repeating contact with each other. Therefore, solid particles interact with each other through these contact forces. Cundal and Strack [15] modelled these forces by springs, dashpots and friction sliders as shown in Figure 10. In our analysis, contact forces between particles each other and/or between particles and a wall are calculated by this discrete element model, and the motion of a particle is computed in a Lagrangian manner by ordinary Newton's equation of motion:

$$m\dot{\mathbf{v}}_p = \mathbf{F} \tag{27}$$

$$\mathbf{F} = \mathbf{f}_C + \mathbf{f}_D + \mathbf{f}_G \tag{28}$$

where $\mathbf{f}_C$ is the contact force, $\mathbf{f}_D$ is the fluid force and $\mathbf{f}_G$ is the gravity force.

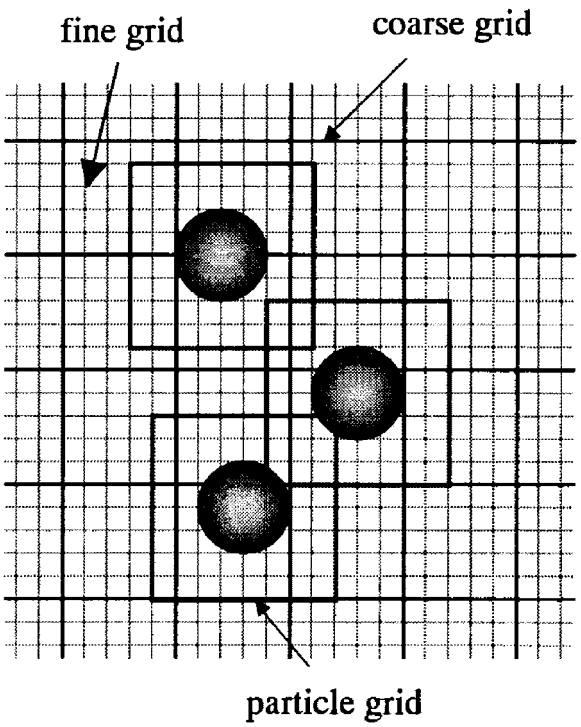

Figure 9. Three kinds of grid.

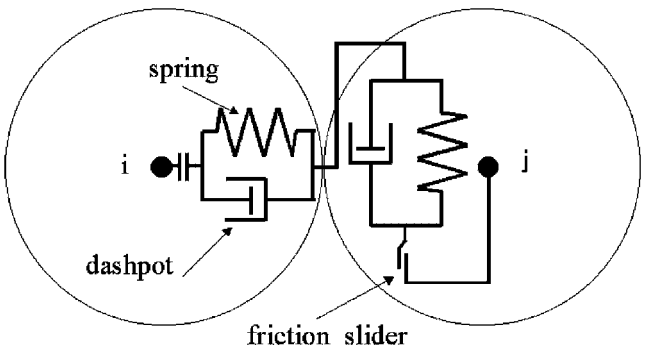

Figure 10. Discrete element model.

As for rotational motion of particles, we assume that only the contact forces affect the motion. Therefore, in terms of moment caused by the contact forces M and inertia moment I, the governing equation of rotational motion is given by

$$I\dot{\omega} = M \tag{29}$$

Integrating Equations (27) and (29), we can compute the velocity $\mathbf{v}_p^{n+1}$ and angular velocity $\boldsymbol{\omega}^{n+1}$ of a particle at the next time step as follows:

$$\mathbf{v}_p^{n+1} = \mathbf{v}_p^n + \dot{\mathbf{v}}_p \Delta t \tag{30a}$$

$$\omega^{n+1} = \omega^n + \dot{\omega} \Delta t \tag{30b}$$

Integrating Equation (30a) with respect to time, the position of a particle $\mathbf{r}^{n+1}$ can be obtained by

$$\mathbf{r}^{n+1} = \mathbf{r}^n + \mathbf{v}_p^n \Delta t \tag{31}$$

It is noted here that the angular velocity ω is used to calculate the tangential component of a contact force.

3.3. *Computational results*

The region of interest is a fluidized bed with an internal heated cylinder as shown in Figure 11. The inputs parameters used in the present analysis are summarized in Table I. Regarding the number of particles, 1548 particles in case of particle diameter 4.76 mm or 538 particles in case of 7.94 mm are disposed so as to realize nearly the same initial thickness of particle layer. As the density of a particle is somewhat small compared with the working fluid, a honeycomb structure is placed at the upper end of the test section to prevent particles from leaving out of this region. The working fluid (water) flows in the region from the upper

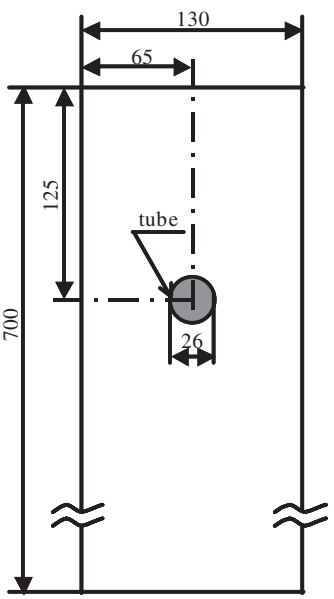

Figure 11. Region of analysis (all in mm unit).

Table I. Analysis condition.

Particle (TPX)	
Diameter	7.94 mm 4.76 mm
Density	833 kg/m^3
Number	538 (7.94 mm) 1548 (4.76 mm)
Fluid (water)	
Density	1000 kg/m^3
Viscosity	10^{-3} Pa*s
Flow passage	
Width	0.13 m
Height	0.70 m
Calculation	
Time increment	0.001 s
Cell size	2×2 mm

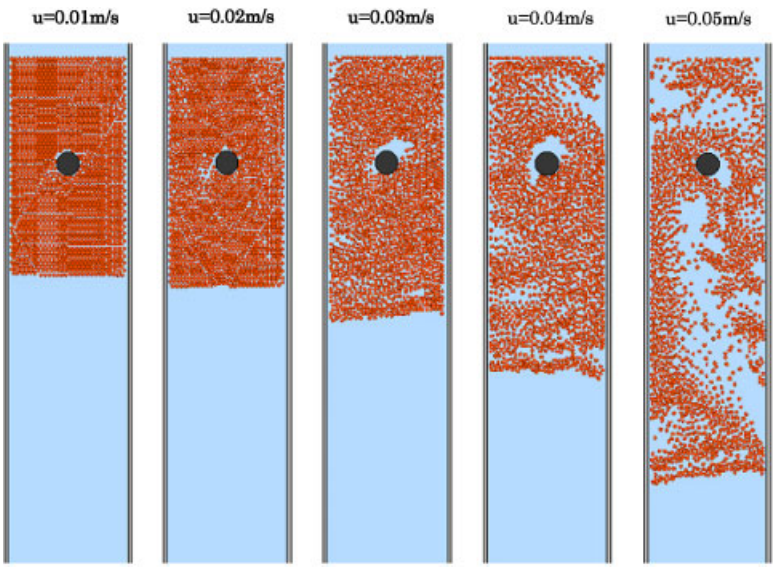

Figure 12. Particles motion at various inlet fluid velocity (dp = 4.76 mm).

boundary. The change in the particle behaviour with the increase of the inlet fluid velocity is shown in Figure 12. From these figures, it is seen that the motion of particles becomes active as the inlet fluid velocity increases and fluidization initiates at the inlet fluid velocity

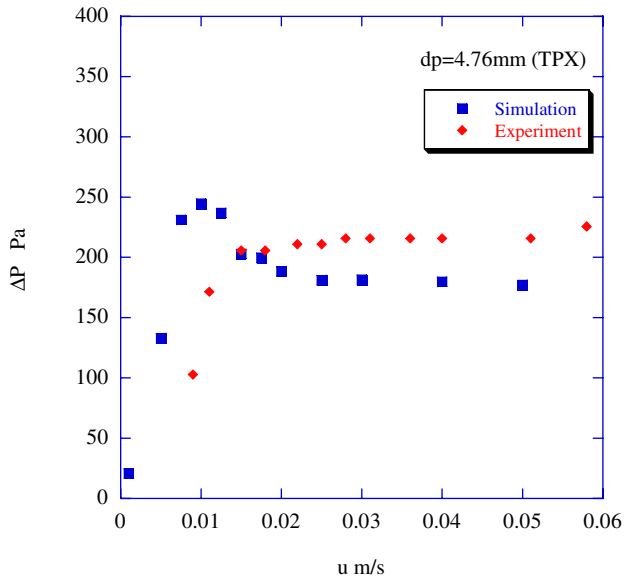

Figure 13. Pressure drop in fluidized bed.

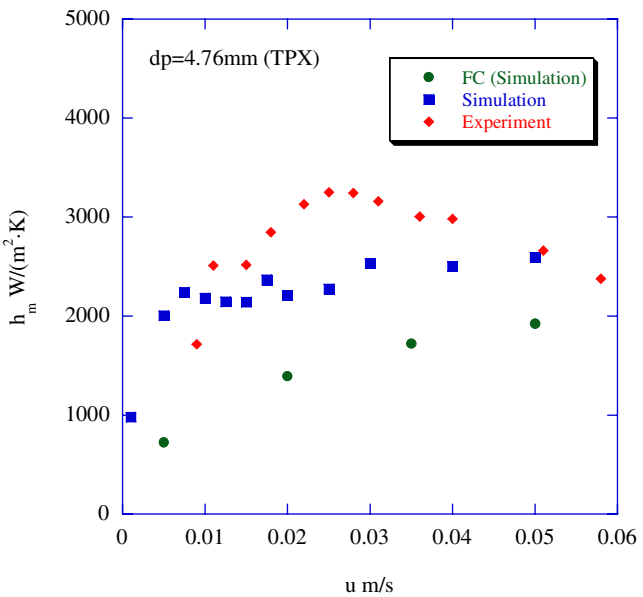

Figure 14. Average heat transfer coefficient on a heated cylinder surface.

of more than 0.02 m/s. In Figure 13, the change of pressure drop with the increase of inlet fluid velocity is illustrated, compared with experimental results obtained in our laboratory. It is confirmed experimentally that after starting fluidization, the pressure drop settles down to

nearly the same level, irrespective of the inlet velocity. The computed results in Figure 13 agree well with these experimental results.

Figure 14 shows the average heat transfer coefficient on the surface of a heated cylinder that is calculated for various inlet fluid velocities. Solid circles denote the heat transfer coefficient for pure forced convection without particles. Although the present analyses are two-dimensional analyses, the enhancement of heat transfer due to fluidization is clearly shown in this figure.

It is noted here that the extension of this method to a three-dimensional problem is straightforward.

4. CONCLUSIONS

A three-dimensional parallel LES technique for viscous incompressible flow with heat transfer using tetrahedral finite-elements and a two-dimensional Voxel method combined with the discrete element method for liquid–solid two-phase flow are presented in this paper. Numerical examples for both methods show good agreement with those of other researchers and the experimental results. These two methods are completely different approaches for large-scale heat transfer and fluid flow problems, however both of these two approaches have proved to be powerful tools for the analysis of realistic large-scale heat transfer problems.

REFERENCES

1. Johnson AA, Tezduyar TE. Parallel computation of incompressible flows with complex geometries. *International Journal for Numerical Methods in Fluids* 1997; **24**:1321–1340.
2. Chan CT, Anastasiou K. An automatic tetrahedral mesh generation scheme by the advancing front method. *Communications in Numerical Methods in Engineering* 1997; **13**:33–46.
3. Patankar SV. *Numerical Heat Transfer and Fluid Flow*. McGraw-Hill: New York, 1980.
4. Gresho PM, Chan ST, Lee RL, Upson CD. A modified finite element method for solving the time-dependent incompressible Navier–Stokes equations. *International Journal for Numerical Methods in Fluids* 1984; **4**: 557–598.
5. Farhat C, Lesoinne M. Automatic partitioning of unstructured meshes for the parallels solution of problems in computer mechanics. *International Journal for Numerical Methods in Engineering* 1993; **36**:745–764.
6. Kawaguchi T, Tanaka T, Tsuji Y. Numerical simulation of two-dimensional fluidized beds using the discrete element method. *Powder Technology* 1998; **96**(2):129–138.
7. Johnson AA, Tezduyar TE. Simulation of multiple spheres falling in a liquid-filled tube. *Computer Methods in Applied Mechanics and Engineering* 1996; **134**:351–373.
8. Johnson A, Tezduyar TE. Advanced mesh generation and update methods for 3D flow simulations. *Computational Mechanics* 1999; **23**:130–143.
9. Johnson A, Tezduyar TE. Methods for 3D computation of fluid-object interactions in spatially-periodic flows. *Computer Methods in Applied Mechanics and Engineering* 2001; **190**:3201–3221.
10. Donea J, Giuliani S, Laval H. Finite element solution of the unsteady Navier–Stokes equations by a fractional step method. *Computer Methods in Applied Mechanics and Engineering* 1982; **30**:53–73.
11. De Vahl Davis G. Natural convection of air in a square cavity. *International Journal for Numerical Methods in Fluids* 1983; **3**:249–264.
12. Le Quere P. Accurate solutions to the square thermally driven cavity at high Rayleigh number. *Computers Fluids* 1991; **20**(1):29–41.
13. Gomes JLMA, Pain CC, de Oliveira CRE, Goddard AJH. Heat transfer models for gas–solid fluidized beds with internals. *Proceedings of the First MIT Conference on Computational Fluid and Solid Mechanics*, 2001; 1199–1204.
14. Anderson TB, Jcakson R. A fluid mechanical description of fluidized beds. *I and EC Fundamentals* 1967; **6**(4):527–539.
15. Cundall PA, Strack ODL. *Geotechnique* 1979; **29**(1):47–65.

